Impedance Matching to Maximize Induced Current in Repeater of Resonant Inductive Coupling Wireless Power Transfer Systems

Masataka Ishihara, Kazuhiro Umetani, Eiji Hiraki
Graduate School of Natural Science and Technology
Okayama University
Okayama, Japan

Published in: 2018 IEEE Energy Conversion Congress and Exposition (ECCE)

DOI: 10.1109/ECCE.2018.8557827

Impedance Matching to Maximize Induced Current in Repeater of Resonant Inductive Coupling Wireless Power Transfer Systems

Masataka Ishihara
Graduate School of Natural Science and Technology
Okayama University
Okayama, Japan
p4wv0vf6@s.okayama-u.ac.jp

Kazuhiro Umetani
Graduate School of Natural Science and Technology
Okayama University
Okayama, Japan
umetani@okayama-u.ac.jp

Eiji Hiraki
Graduate School of Natural Science and Technology
Okayama University
Okayama, Japan
hiraki@okayama-u.ac.jp

***Abstract*— Intermediate resonators (repeaters) of resonant inductive coupling wireless power transfer systems can improve the transmission distance as well as the output power. However, frequency bandwidths in which the repeater can operate effectively are very narrow because the repeater usually has a high quality-factor. Furthermore, these frequency bandwidths shift for the following two factors. The first factor is the intensity of the magnetic coupling between the repeater and the other resonator. The second factor is the variation in the natural resonance frequency of the resonators due to a production error, temperature characteristic, and aging degradation. Therefore, the repeater is not practical because the repeater requires accurate adjusting of the circuit parameters every time according to the various conditions. To address this problem, we propose an impedance matching method for the repeater. The proposed method can maximize the induced current in the repeater in wide frequency bandwidth regardless of the variations in the intensity of the magnetic coupling and the natural resonance frequency. Therefore, the proposed method can realize the repeater which can stably improve the performance of the wireless power transfer. Experiment and simulation successfully verified the effectiveness of the proposed method as well as the appropriateness of the theoretical analysis.**

Keywords—wireless power transfer, resonant inductive coupling, repeater, impedance matching, frequency splitting phenomenon

I. INTRODUCTION

Wireless power transfer (WPT) techniques can transfer electric power without physical cable connections. As a result, the WPT techniques realize a convenient, reliable, and safe power supply. Resonant inductive coupling WPT (RIC-WPT) systems are widely studied as a high efficiency WPT technique for various battery powered applications. The RIC-WPT can transfer the electric power via a vacant space using the magnetic coupling between coils. For low power applications such as home appliances [1], mobile apparatus [2], implantable medical devices [3], it is required to transfer enough power even if the transmission distance of the WPT increases so as not to damage convenience.

However, the RIC-WPT for the low power applications often suffer from the short transmission distance because the size of receiving resonator (receiver) is usually limited due to small installation area [4]. The small-sized receiver tends to be difficult to ensure the enough magnetic coupling. Therefore, improving the transmission distance is the key issue and urgent demand in order for the RIC-WPT for the low power applications to become more practical.

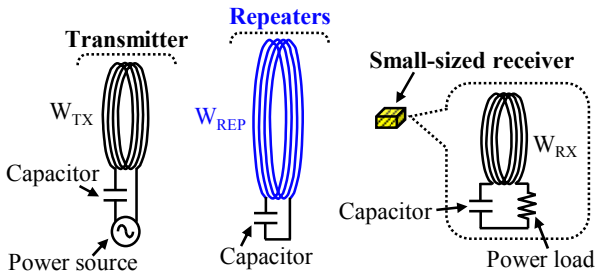

Fig. 1. Resonant inductive coupling wireless power transfer (RIC-WPT) system with repeater.

As a method to approach this problem, adding an intermediate resonator (repeater) has been widely studied [1, 4–9]. The repeater is utilized by placing near the transmitting resonator (transmitter) as shown in Fig. 1, where W_{TX}, W_{REP}, and W_{RX} represent the transmitting, repeating, and receiving coils, respectively. The role of the repeater is to relay the magnetic field from the transmitter to the receiver [5]. In some case, multiple repeaters are used to further expand the transmission distance [7, 8]. The quality-factor (Q-factor) of the repeater is generally as large as several hundreds because the repeater consists of only the passive components. Therefore, in principle, a large current in the repeater can be easily induced even if the intensity of the magnetic coupling is weak [9]. By inducing a large current in the repeater, the repeater can enhance the magnetic field far from the transmitter. As a result, the repeater can improve the transmission distance between the transmitter and the receiver.

However, in fact, it is often difficult to induce a large current in the repeater due to troublesome frequency characteristics of the repeater. The repeater having a high Q-factor often suffers from frequency splitting phenomenon [5, 6, 9–13]. This phenomenon easily occurs when the Q-factor of resonators is high even if the intensity of the magnetic coupling is weak [9, 10]. The frequency characteristic of the induced current in the repeater has multiple peaks when the frequency splitting phenomenon occurs [5, 6, 9–13]. In addition, the peaks are very sharp because the Q-factor is high. Consequently, the frequency bandwidths in which a large current can be induced to the repeater, namely, the frequency bandwidths in which the repeater can operate effectively are very narrow. Moreover, these narrow frequency bandwidths shift for the following two factors: (i) the intensity of the magnetic coupling between the repeater and the other resonator depending on the relative location of the repeater [5, 6, 9, 10, 13–16], (ii)

a few percent variation in the natural resonance frequency of the resonator due to a production error, temperature characteristic, and aging degradation [9, 14, 17]. Hence, the repeater is not practical because the magnitude of the induced current in the repeater is highly dependent on the above two factors. Consequently, the resonance frequency of the resonator must be adjusted every time according to the various conditions so that either of the frequency corresponding to the peaks is close to the operating frequency.

However, even if the resonance frequency is properly adjusted, based on the concept of the impedance matching, the induce current in the repeater cannot be maximized unless the equivalent resistance of the repeater viewed from the transmitting side (the real part of reflected impedance [3, 18] of the repeater) is properly adjusted. Recently, in order to adjust the equivalent resistance viewed from the transmitting side, several impedance matching methods have been proposed using DC-DC converter [19, 20] or active rectifier [14, 21]. However, these impedance matching methods are originally proposed for the receiver having the load resistance. Therefore, these impedance matching methods cannot be applied to the repeater because the repeater has not the load resistance.

Therefore, the purpose of this paper is to propose the impedance matching method for the repeater. The proposed impedance matching method can maximize the induced current in the repeater in wide frequency bandwidth regardless of the variations in the intensity of the magnetic coupling and the natural resonance frequency. The basic idea of the proposed impedance matching method is an auxiliary circuit named an automatic tuning assist circuit (ATAC) originally proposed in [17]. The ATAC is an attractive technique because the ATAC can adjust the phase of the current in the resonator, namely, the resonance frequency of the resonator without complicated control [9, 17]. Reference of [17] has reported the effectiveness of the ATAC applied to the transmitter under the limited condition in which the frequency splitting phenomenon does not occur. Then, our previous study [9] has been verified the effectiveness the ATAC under the condition in which the frequency splitting phenomenon occurs. According to [9], the ATAC applied to the repeater can realize the repeater which is less affected by the variation in the intensity of the magnetic coupling. However, in [9], the induced current in the repeater cannot be maximized because the optimal impedance matching has not been achieved. In other words, the approach reported in [9] can adjust the resonance frequency of the repeater, however the equivalent resistance of the repeater viewed from the transmitting side cannot be adjusted. On the other hand, the impedance matching method proposed in this paper can adjust not only the resonance frequency of the repeater but also the equivalent resistance of the repeater viewed from the transmitting side.

The following discussion consists of four sections. Section II presents a brief review of the basic operation principle of the ATAC in order to discuss the proposed impedance matching method. Then, section III elucidates that the proposed impedance matching method can maximize the induced current in the repeater. Section IV presents experimental results to verify the effectiveness of the proposed impedance matching method and appropriateness of the theoretical analysis. Finally, section V gives conclusions.

II. Operating Principle of ATAC

In this section, based on [9, 17], we review the operating principle of the ATAC by using the basic circuit shown in Fig. 2. This circuit comprises the AC voltage source V_s, the resonator (composed of the coil L, the capacitor C, and the parasitic resistor r), and the ATAC. The ATAC consists of the full-bridge circuit. The DC bus line of the full-bridge circuit has only the smoothing capacitor C_A. The capacitance of C_A does not contribute to the resonance frequency of the resonator because it is sufficiently greater than the capacitance of C.

The switches Q_1–Q_4 of the ATAC are turned on or off in synchronization with V_s and with an arbitrary phase difference φ with respect to V_s as shown in Fig. 3 (a). In addition, the DC voltage appears in C_A when Q_1–Q_4 start operating. Therefore, the ATAC generates the rectangular wave voltage using the self-generated DC voltage. As a result, the ATAC can be expressed as the AC voltage source as shown in Fig. 4, where V_A is the effective value of the fundamental wave component of the rectangular voltage generated by the ATAC. When the Q-factor of the resonator is sufficiently larger than 1, the rectangular voltage can be approximated as the sinusoidal voltage [12].

As shown in Fig. 5, the current I_L in the resonator is the superposition of the current I_s generated by V_s and the current I_A generated by $-V_A$. The definitions of I_L and V_A are in opposite directions. Therefore, in Fig. 5, the sign of V_A is

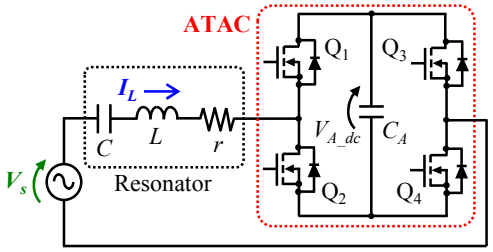

Fig. 2. Single resonator with ATAC.

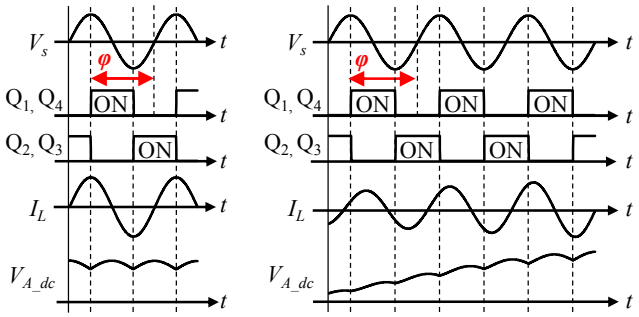

(a) Steady state (b) transient state

Fig. 3. Schematic diagram of operating waveforms of ATAC.

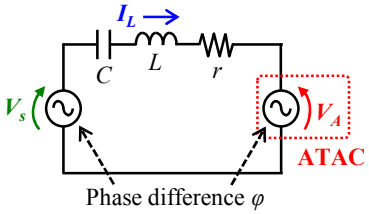

Fig. 4. Equivalent circuit of Fig. 2.

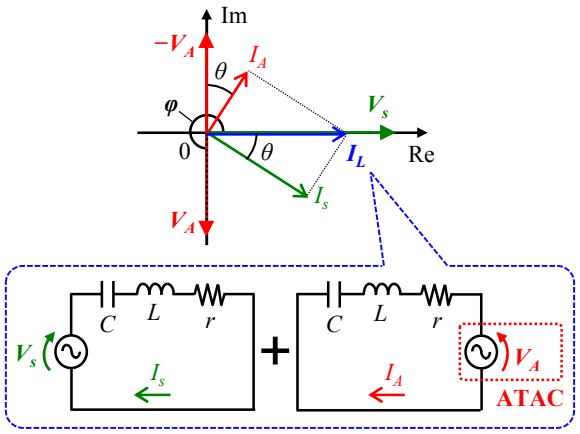

Fig. 5. Phasor diagram of Fig 4 in steady state.

negative. I_s is the current when the ATAC is not applied. Hence, the phase difference θ between V_s and I_s shown in Fig. 5 is uniquely determined by the impedance of the resonator and the operating frequency of V_s. Therefore, the phasor of I_L can be changed according to the phasor of I_A.

The ATAC does not ideally dissipate effective power because the ATAC does not have any resistive component. Therefore, the phase difference between V_A and I_L shown in Fig. 5 is always $\pi/2$. In other words, the time integrations of the current for charging and discharging C_A must be equal with each other as shown in Fig. 3 (a). The magnitude of V_A is automatically determined so that the phase difference between V_A and I_L is $\pi/2$. Hence, the phase of I_L can be freely controlled by only setting phase difference φ between V_A and V_s regardless of the impedance of the resonator and the operating frequency of V_s. In particular, in the phasor diagram of Fig. 5, when φ is set to $3\pi/2$ ($-\pi/2$), the imaginary part of I_L is fully canceled, and the resonator works as a resistive circuit.

However, the range of φ that the ATAC can operate is limited as pointed in [9, 17]. To generate a DC voltage in C_A, in the initial operation, the time integrations of the current for charging the C_A must be larger than the time integrations of discharging, as shown in Fig. 3 (b). Therefore, when we apply the ATAC to the inductive resonator as shown Fig. 5, the phase difference φ must be set to $3\pi/2 \le \varphi \le 2\pi$ ($-\pi/2 \le \varphi \le 0$). On the other hand, when we apply the ATAC to the capacitive resonator, the phase difference φ must be set to $0 \le \varphi \le \pi/2$.

Moreover, the switches of the ATAC can achieve the Zero-voltage-switching (ZVS) turn-on when the phase of I_L is delayed by $\pi/2$ with respect to $-V_A$ in the steady state. However, the switches of the ATAC operate under hard-switching (HS) turn-on when the phase of I_L is advanced by $\pi/2$ with respect to $-V_A$ in the steady state. The switches should operate under the ZVS turn-on because the HS turn-on equivalently decreases the Q-factor of the resonator due to the switching loss.

III. Impedance Matching Method to Maximize Induced Current in Repeater

The purpose of this section is to present how the proposed impedance matching method maximizes the induced current in the repeater. In addition, we formulate characteristics in the steady state of the proposed system.

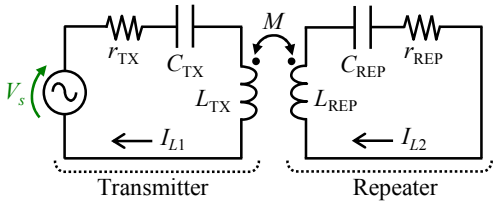

Fig. 6. Simplified equivalent circuit of Fig. 1.

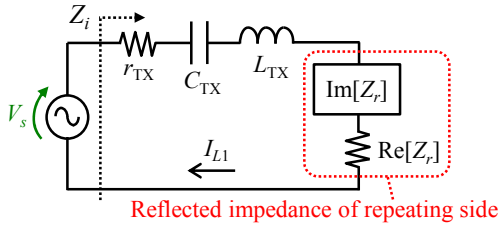

Fig. 7. Equivalent circuit with reflected impedance of Fig. 6.

A. Conventional RIC-WPT System (without Proposed Impedance Matching Method)

Firstly, we analyze the conventional RIC-WPT system not applying the proposed impedance matching method shown in Fig. 1. Then, we indicate why it is difficult to maximize the current in the repeater. Figure 6 illustrates the simplified equivalent circuit of Fig. 1, where V_s is the voltage of the AC voltage source, L_{TX} and L_{REP} are the self-inductance of W_{TX} and W_{REP}, respectively, C_{TX} and C_{REP} are the capacitance of the resonance capacitor, r_{TX} and r_{REP} are the series parasitic resistance of the transmitter and the repeater, respectively, and M is the mutual inductance between W_{TX} and W_{REP}. In this paper, the small-sized receiver is ignored because the small-sized receiver usually uses only little flux to receive the power. Therefore, we assume the small-sized receiver does not affect to the currents in the transmitter and the repeater.

According to Kirchhoff's voltage law, Fig. 6 can be described as

$$\begin{aligned} V_s &= (r_{TX}+jX_{TX})I_{L1} - j\omega M I_{L2}, \\ j\omega M I_{L1} &= (r_{REP}+jX_{REP})I_{L2}, \end{aligned} \tag{1}$$

where jX_{TX} and jX_{REP} are expressed as

$$\begin{aligned} jX_{TX} &= j(\omega L_{TX} - 1/\omega C_{TX}), \\ jX_{REP} &= j(\omega L_{REP} - 1/\omega C_{REP}). \end{aligned} \tag{2}$$

The repeating side can be modeled as reflected impedance Z_r [3, 18] on the transmitting side as shown in Fig. 7. As pointed out in [3, 18], based on (1) and (2), the real part of the Z_r (the equivalent resistance of the repeater viewed from the transmitting side) and the imaginary part of the Z_r can be obtained respectively as

$$\begin{aligned} \mathrm{Re}[Z_r] &= \omega^2 M^2 r_{REP} / \left(X_{REP}^2 + r_{REP}^2\right), \\ \mathrm{Im}[Z_r] &= -\omega^2 M^2 X_{REP} / \left(X_{REP}^2 + r_{REP}^2\right). \end{aligned} \tag{3}$$

In order to maximize the induced current in the repeater, the power consumed by Re[Z_r] in Fig. 7 have to maximize. Therefore, based on the concept of the impedance matching,

the current in the repeater of Fig. 6 can be maximized by satisfying the following two conditions. The first condition is to achieve the relationship of r_{TX}=Re[Z_r] by adjusting X_{REP}. The second condition is to set the reactance component (the imaginary part) of the input impedance Z_i to zero by adjusting X_{TX}. However, in order to achieve these two conditions, it is necessary to accurately estimate r_{TX}, r_{REP}, and M when adjusting Re[Z_r] because both Re[Z_r] and Im[Z_r] depend on X_{REP}. Hence, it is often difficult to maximize the induced current in the repeater according to the various situations.

Then, in order to compare the conventional system with the proposed system in the section IV, we formulate characteristics of I_{L1} and I_{L2} based on [9, 14]. By substituting (2) into (1), I_{L1} and I_{L2} can be derived accordingly as

$$\begin{aligned} I_{L1} &= V_s(N_{1R}+jN_{1I})/D_p\,, \\ I_{L2} &= V_s(N_{2R}+jN_{2I})/D_p\,, \end{aligned} \tag{4}$$

where N_{1R}, N_{1I}, N_{2R}, N_{2I}, and D_p are defined as

$$\begin{aligned} N_{1R} &= \omega^2M^2r_{REP}+r_{TX}\left(r_{REP}^2+X_{REP}^2\right), \\ N_{1I} &= \omega^2M^2X_{REP}-X_{TX}\left(r_{REP}^2+X_{REP}^2\right), \\ N_{2R} &= \omega M(X_{TX}r_{REP}+X_{REP}r_{TX}), \\ N_{2I} &= \omega M\left(\omega^2M^2+r_{TX}r_{REP}-X_{TX}X_{REP}\right), \\ D_p &= 2\omega^2M^2\left\{r_{TX}r_{REP}-X_{TX}X_{REP}+\omega^2M^2/2\right\} \\ &\quad +\left(r_{TX}^2+X_{TX}^2\right)\left(r_{REP}^2+X_{REP}^2\right). \end{aligned} \tag{5}$$

B. *RIC-WPT System with Proposed Impedance Matching Method*

Then, Fig. 8 shows the equivalent circuit of the RIC-WPT system with the proposed impedance matching method, where κ is a proportional constant, V_{A1} and V_{A2} are the voltage of the ATAC of the transmitting and repeating side, respectively. In the proposed system, the ATAC is applied to each of the transmitter and the repeater. Fig. 9 shows the phasor diagram of Fig. 8. The ATAC on the transmission side is driven with the phase difference fixed to $\pi/2$ with respect to V_s. On the other hand, the ATAC on the repeating side is driven with the phase difference θ to with respect to V_s. According to the discussion of the previous section, the phase difference between V_{A1} and I_{L1} as well as V_{A2} and I_{L2} are always $\pi/2$, respectively. In addition, based on Fig. 9. the both ATACs can achieve the ZVS turn-on.

According to Kirchhoff's voltage law, Fig. 8 can be described as

$$\begin{aligned} V_s+jV_{A1} &= (r_{TX}+jX_{TX})I_{L1} \\ &\quad -j\omega M\kappa V_{A2}(-\sin\theta+j\cos\theta), \\ j\omega MI_{L1} &= (r_{REP}+jX_{REP})\kappa V_{A2}(-\sin\theta+j\cos\theta) \\ &\quad +V_{A2}(\cos\theta+j\sin\theta). \end{aligned} \tag{6}$$

Similarly, as in Fig. 7, the repeating side can be modeled as the reflected impedance on the transmitting side as shown in Fig. 10. Based on (2) and (6), Re[Z_r] and Im[Z_r] of Fig. 10 can be obtained respectively as

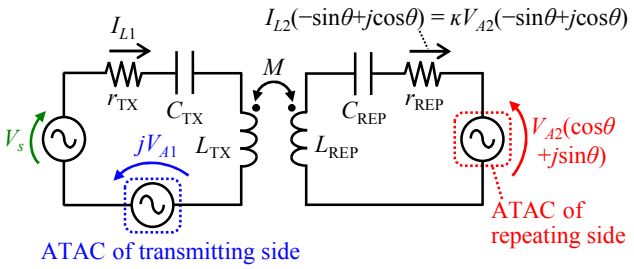

Fig. 8. RIC-WPT system with proposed impedance matching method.

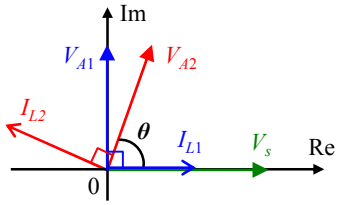

Fig. 9. Phasor diagram of Fig. 8 in steady state.

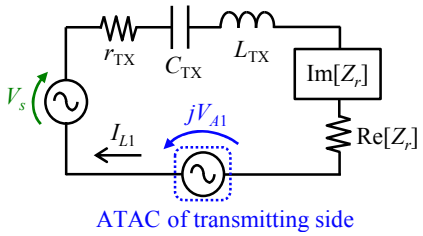

Fig. 10. Equivalent circuit with reflected impedance of Fig. 8.

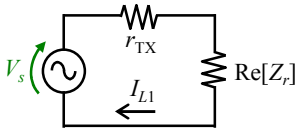

Fig. 11. Equivalent circuit of Fig. 10 transformed based on operating principle of ATAC.

$$\begin{aligned} \mathrm{Re}[Z_r] &= (\omega M\cos\theta)^2/r_{REP}\,, \\ \mathrm{Im}[Z_r] &= \omega^2M^2\cos\theta\sin\theta/r_{REP}\,. \end{aligned} \tag{7}$$

In the conventional system of Fig. 6, the reflected impedance Z_r is adjusted by setting X_{REP}. On the other hand, according to (7), the reflected impedance Z_r can be controlled by setting θ in the proposed system of Fig. 8.

Based on the operating principle of the ATAC described in the previous section, the reactive current caused by the reactance components in the equivalent circuit of Fig. 10 can be canceled by the ATAC of the transmission side. Consequently, Fig. 10 can be transformed to Fig. 11. In order to maximize the induced current in the repeater, θ should be set to satisfy the relationship of r_{TX}=Re[Z_r]. In the range of $-\pi<\theta<\pi$, θ_{opt} which can maximize the induce current in the repeater can be obtained as

$$\theta_{opt} = \pm\cos^{-1}\left(1/k\sqrt{Q_{TX}Q_{REP}}\right), \tag{8}$$

where k is the coupling coefficient, i.e. $k^2=M^2/L_{TX}L_{REP}$; Q_{TX} and Q_{REP} are the Q-factor of the transmitter and the repeater, respectively, i.e. $Q_{TX}=\omega L_{TX}/r_{TX}$ and $Q_{REP}=\omega L_{REP}/r_{REP}$. In order for the solution of θ_{opt} to exist, the relationship of $k^2Q_{TX}Q_{REP}\geq1$ must be satisfied. The relationship of

$k^2Q_{TX}Q_{REP}\geq 1$ is the same as the condition under which the frequency splitting phenomenon occurs [10].

From (8), θ_{opt} has two solutions according to the sign of plus or minus. The phase of the induced current in the repeater is different depending on the sign of the θ_{opt} as shown in Fig. 9. Another advantage of the proposed impedance matching method is that the resonance modes [10, 11] of the repeater can be selected by only selecting the sign of θ_{opt}. When the sign of θ_{opt} is set to positive, the repeater operates as the odd mode. On the other hand, when the sign of θ_{opt} is set to negative, the repeater operates as the even mode. The magnetic field distribution generated by the transmitter and the repeater differs according to the resonance modes [10]. Therefore, it is necessary to select the resonance mode depending on the location of the receiver.

In the proposed impedance matching method, the ATAC automatically compensates for the variations in the natural resonance frequency of the transmitter and the repeater. Therefore, the induced current in the repeater can be maximized regardless of the variation in the natural resonance frequency. However, the voltage of the ATAC (V_{A1} and V_{A2}) tends to increase as the variation in the natural resonance frequency increases. Moreover, the proposed impedance matching method can eliminate the difficulty due to the frequency splitting phenomenon because Im[Z_r] which is the cause of the frequency splitting phenomenon can be canceled by the ATAC of the transmitting side.

Finally, we formulate characteristics of the proposed system shown in Fig. 8. By substituting (8) into (6), I_{L1} and I_{L2} at $\theta=\pm\theta_{opt}$ can be derived accordingly as

$$I_{L1}|_{\theta=\pm\theta_{opt}}=V_s/2r_{TX}\,,\quad I_{L2}|_{\theta=\pm\theta_{opt}}=V_s/2\sqrt{r_{TX}+r_{REP}}. \tag{9}$$

Equation (9) indicates that the magnitude of the current in the repeater and the transmitter does not depend on the resonance frequencies of the resonators. Similarly, as in (9), V_{A1} and V_{A2} at $\theta=+\theta_{opt}$ can be obtained as

$$V_{A1}|_{\theta=+\theta_{opt}}=\frac{X_{TX}+r_{TX}\sqrt{k^2Q_{TX}Q_{REP}-1}}{2r_{TX}}V_s, \tag{10}$$

$$V_{A2}|_{\theta=+\theta_{opt}}=\frac{X_{REP}+r_{REP}\sqrt{k^2Q_{TX}Q_{REP}-1}}{2\sqrt{r_{TX}+r_{REP}}}V_s. \tag{11}$$

Then, V_{A1} and V_{A2} at $\theta=-\theta_{opt}$ can be derived accordingly as

$$V_{A1}|_{\theta=-\theta_{opt}}=\frac{X_{TX}-r_{TX}\sqrt{k^2Q_{TX}Q_{REP}-1}}{2r_{TX}}V_s, \tag{12}$$

$$V_{A2}|_{\theta=-\theta_{opt}}=\frac{X_{REP}-r_{REP}\sqrt{k^2Q_{TX}Q_{REP}-1}}{2\sqrt{r_{TX}+r_{REP}}}V_s. \tag{13}$$

IV. Experimetal Results

In this section, experiment and simulation are carried out to verify that the proposed impedance matching method can maximize the induced current in the repeater regardless of the variations in the intensity of the magnetic coupling and natural resonance frequency. In addition, we verify the appropriateness of the theoretical analysis results in the previous section by the experiment and the simulation.

Figure 12 illustrates the circuit configuration for the experiment and the simulation. Moreover, Fig. 13 shows the photograph of the experimental setup of the proposed system. In order to drive the ATAC of the repeating side, it is necessary to self-generate the power and the control signal to drive the switches constituting the ATAC because the repeater does not have any power sources. In addition, the phase difference θ of the ATAC applied to the repeater must be controlled to either $+\theta_{opt}$ or $-\theta_{opt}$. However, these are out of the scope of this paper. Therefore, in this paper, the ATACs are driven by using the external power supply and the signal generator as shown in Fig. 13. The proposed impedance matching method which can self-drive will be realized by our future works.

Table I shows the circuit parameters for the experiment and the simulation. In this paper, based on Table I, we carry out following three evaluations.

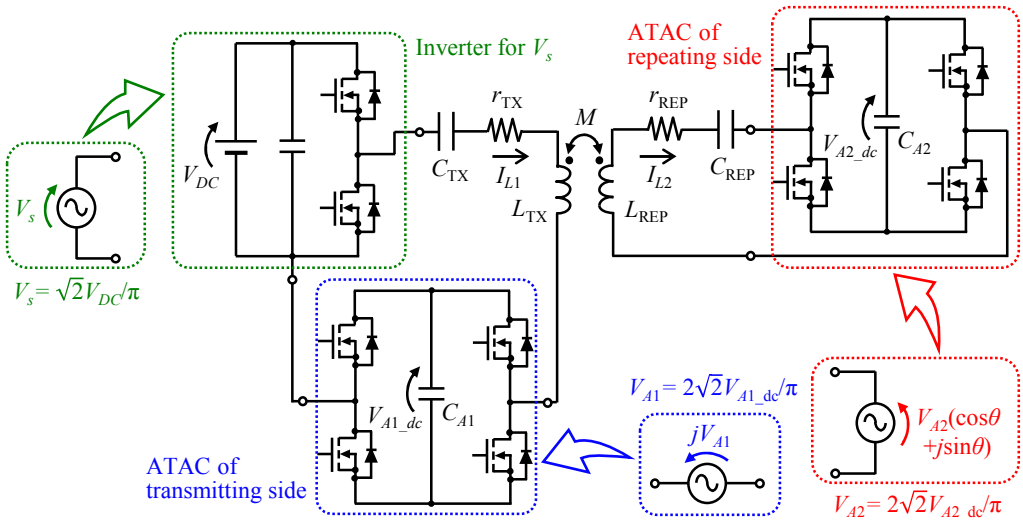

Fig. 12. Circuit configuration for experiment and simulation (with proposed impedance matching method).

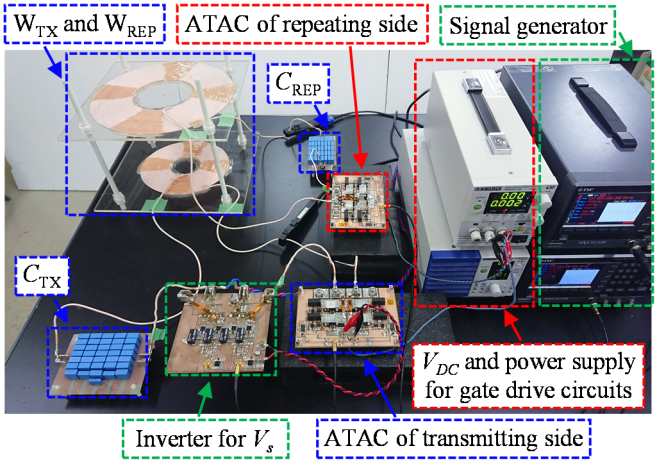

Fig. 13. Photograph of experimental setup.

a) In the first evaluation, we evaluate the frequency characteristics of I_{L1}, I_{L2}, V_{A1_dc}, V_{A2_dc}, and θ_{opt} when the circuit parameters are set to the initial designed value, i.e. C_{REP} is set to 16.14 nF and M is set to 2.30 µH. In the initial designed value, the parameters have been determined such that the resonance frequencies of the transmitter and the repeater are nearly equal. Moreover, in the first evaluation, we evaluate the frequency characteristics under both of $\theta=+\theta_{opt}$ and $\theta=-\theta_{opt}$. Then, based on the experimental and simulation results, we discuss the difference of characteristics between the proposed system and the conventional system. In addition, we verify the appropriateness of the theoretical analysis results in the previous section.

b) In the second evaluation, we set C_{REP} to 15.34 nF which is 5% smaller than the initial design value of 16.14 nF. Then, we evaluate the frequency characteristics of I_{L2}, V_{A1_dc}, and V_{A2_dc} and θ_{opt}. The sign of θ_{opt} is set to positive.

TABLE I. CIRCUIT PARAMETERS

Input DC voltage	V_{DC}	4.0 V
Self-inductance of W_{TX}	L_{TX}	55.32 µH
Parasitic resistance of transmitter	r_{TX}	0.107 Ω
Capacitance of transmitter	C_{TX}	40.81 nF
Self-inductance of W_{REP}	L_{REP}	141.62 µH
Parasitic resistance of repeater	r_{REP}	0.171 Ω
Capacitance of repeater (Initial designed value)	C_{REP}	16.14 nF
Mutual inductance (Initial designed value)	M	2.30 µH
Capacitance of ATAC	$C_{A1, A2}$	22 µF
Capacitance of repeater (5% smaller than 16.14 nF)	C_{REP}	15.34 nF
Mutual inductance (2.1 µH larger than 2.30 µH)	M	4.40 µH

Based on this evaluation, we indicate the effectiveness of the proposed impedance matching method.

c) In the third verification, we set M to 4.40 µH which is 2.1 µH larger than the initial design value of 2.30 µH. In this verification, C_{REP} is set to the initial design value, i.e. C_{REP}=16.14 nF. Then, we evaluate the frequency characteristics of I_{L2}, V_{A1_dc}, and V_{A2_dc} and θ_{opt}. The sign of θ_{opt} is set to positive. Based on this evaluation, we indicate the effectiveness of the proposed impedance matching method.

Figures 14 and 15 shows the results of the first evaluation. The phase difference θ is set to $+\theta_{opt}$ in Fig. 14, and θ is set to $-\theta_{opt}$ in Fig. 15. In the experiment, $+\theta_{opt}$ and $-\theta_{opt}$ are defined the phase difference in which I_{L2} becomes a maximum. The results of the conventional system are the same in Fig. 14 and Fig. 15. In order to operate the proposed impedance matching method, the DC voltage of the both ATACs (V_{A1_dc} and V_{A2_dc}) must be positive. Therefore, in the proposed system, the experiments can be carried out at

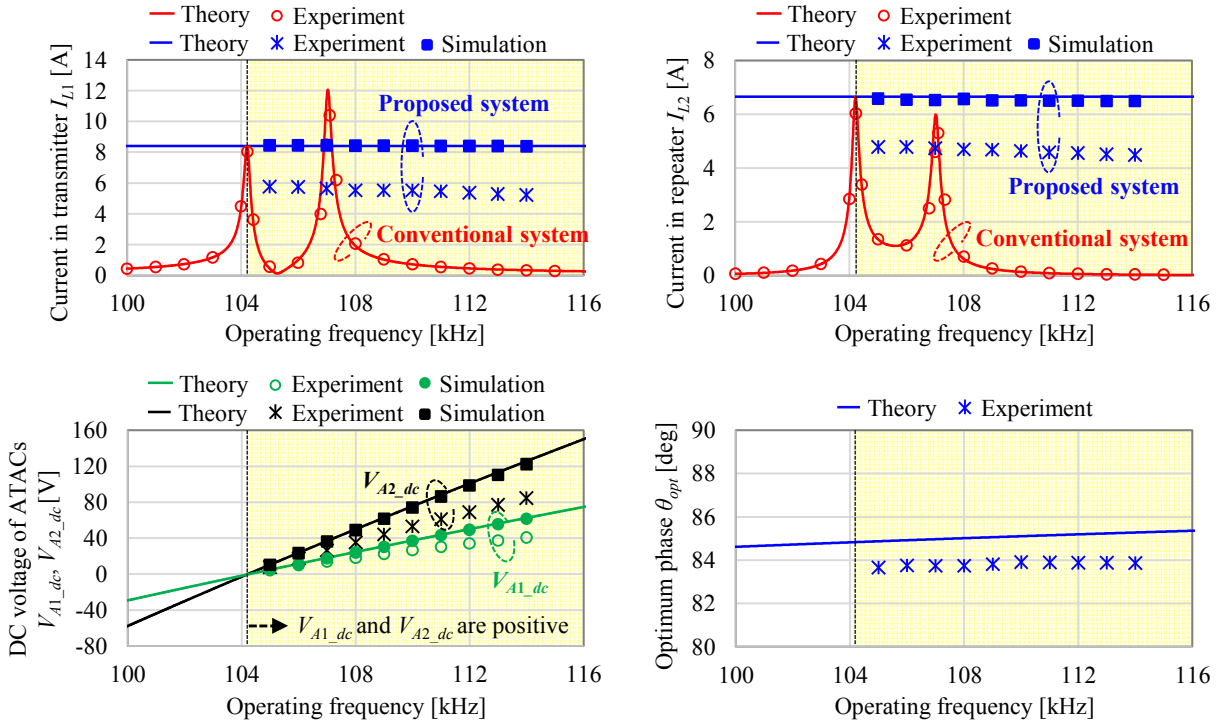

Fig. 14. Frequency characteristics of I_{L1}, I_{L2}, V_{A1_dc}, V_{A2_dc}, and θ_{opt} under initial designed values (Sign of θ_{opt} is set to positive).

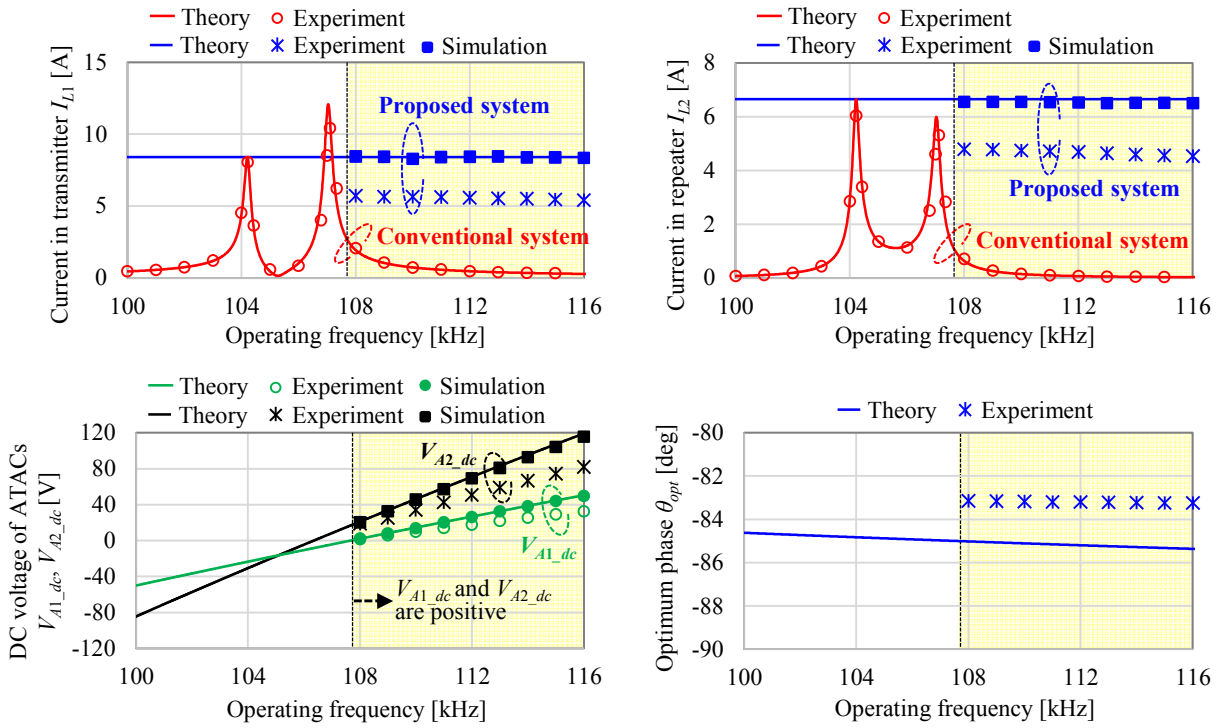

Fig. 15. Frequency characteristics of I_{L1}, I_{L2}, V_{A1_dc}, V_{A2_dc}, and θ_{opt} under initial designed values (Sign of θ_{opt} is set to negative).

only frequencies in which the both V_{A1_dc} and V_{A2_dc} are positive. Furthermore, the upper limit of the operating frequency for the proposed system is determined by the breakdown voltage of the MOS FETs (IPB083N10N3 G manufactured by Infineon Technologies) constituting the ATACs.

As can be seen from Fig. 14 and Fig. 15, in the case of the conventional system, two sharp peaks appear in the frequency characteristics of I_{L1} and I_{L2} due to the frequency splitting phenomenon. It is known that the lower peak corresponds to the odd mode, and the higher peak corresponds to the even mode [10, 11]. From Fig. 14 and Fig. 15, in the case of the conventional system, the frequency bandwidths in which the repeater can operate effectively are very narrow. On the other hand, in the case of either $\theta=+\theta_{opt}$ and $\theta=-\theta_{opt}$, the proposed system can induce almost constant and relatively large current in the repeater in the wide operating frequency bandwidth regardless of the frequency splitting phenomenon.

Form Fig. 14 and Fig. 15, the experimental results are corresponded well with the theoretical values in the case of the conventional system. On the other hand, in the case of the proposed system, the experimental results have some error with respect to the theoretical values. The errors occur because the Q-factor of the resonators used in the experiment are very large. The Q-factors of the initial designed values are $Q_{TX}\approx360$ and $Q_{REP}\approx570$ at 110 kHz. Therefore, the slight losses caused by adding the ATACs easily affect to the experimental results. Based on (9) and experimental results, additional parasitic resistances caused by the ATACs can be roughly calculated. As a result, the Q-factors equivalently decrease to $Q_{TX}\approx245$ and $Q_{REP}\approx430$ at 110 kHz by adding the ATACs. Although the experimental results are lower than the theoretical values, the proposed system can induce large current in the repeater in the wide frequency bandwidth compared with the conventional system. The simulation results without losses of the ATACs are corresponded well with the theoretical values. Therefore, the appropriateness of the theoretical analysis results in the previous section can be confirmed.

Finally, Fig. 16 and 17 shows the results of the second and third evaluations, respectively. From Fig. 16 and 17, in the case of the conventional system, the frequencies at which the peaks of I_{L2} appeared are shifted when there are the variations in the natural resonance frequency and the intensity of the magnetic coupling. Therefore, to design the practical repeater, accurate adjusting of the circuit parameters must be required every time according to the various conditions. On the other hand, from Fig. 14–17, the proposed system can induce I_{L2} of almost same magnitude regardless of the variations of the circuit parameters. In other words, the proposed impedance matching method can eliminate that the performance of the repeater is influenced by the variation in the circuit parameters.

V. Conclusion

The repeater having high Q-factor is effective for improving the transmission distance as well as the output power. However, the performance of the repeater which has high Q-factor is easily affected by the variations in the intensity of the magnetic coupling and the natural resonance frequency. Therefore, the repeater cannot operate effectively without accurate adjusting of the circuit parameters every time according to the various conditions. In order to approach this difficulty, we proposed the impedance matching method for the repeater using the ATACs. The proposed impedance matching method can maximize the induced current by adjusting the real and imaginary parts of the reflected impedance. In addition, the proposed method can select the phase of the current in the repeater corresponding to either of odd mode or even mode by only selecting the sign of the optimum phase difference (θ_{opt}) for the ATAC applied to the repeating side. From the experimental results, it is clarified that although the

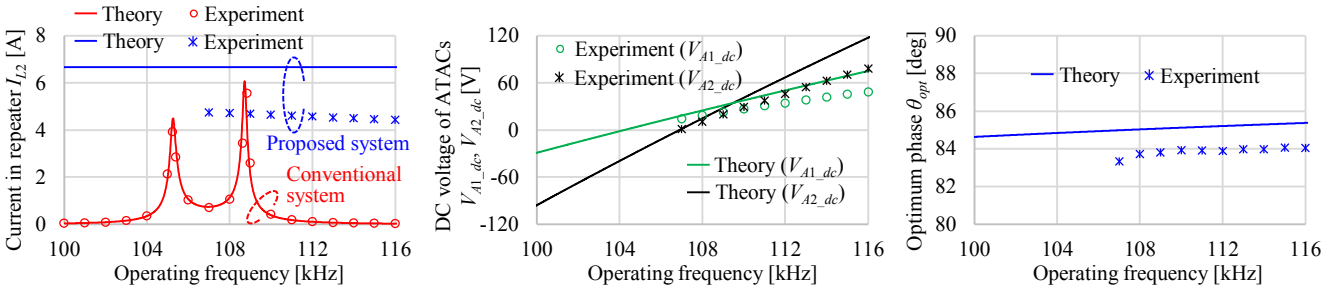

Fig. 16. Frequency characteristics of I_{L1}, I_{L2}, V_{A1_dc}, V_{A2_dc}, and θ_{opt} when C_{REP} is set to 15.34 nF (Sign of θ_{opt} is set to positive).

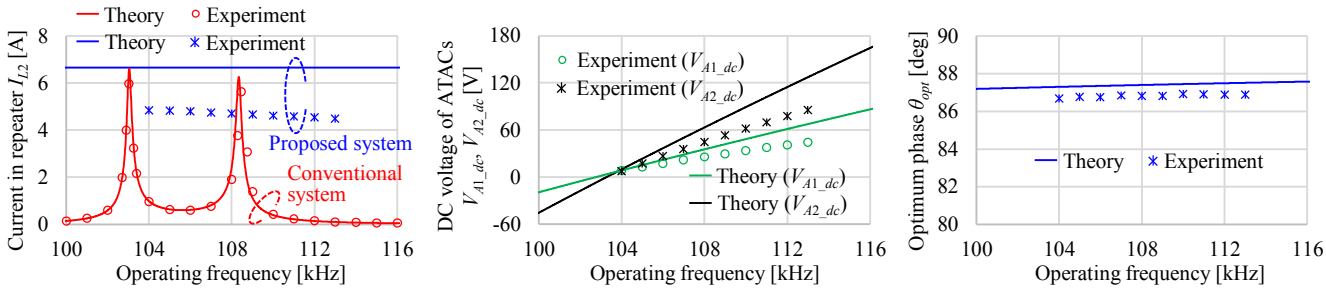

Fig. 17. Frequency characteristics of I_{L1}, I_{L2}, V_{A1_dc}, V_{A2_dc}, and θ_{opt} when M is set to 4.40 μH (Sign of θ_{opt} is set to positive).

proposed method slightly decreases the Q-factor of the resonators, it can stably induce a large current in the repeater in wide frequency bandwidth even if there are the variations in the intensity of the magnetic coupling and the natural resonance frequency. As a result, we conclude that the proposed impedance matching method can realize the repeater which can operate effectively under the various conditions.

REFERENCES

[1] J. Kim, H.-C. Son, D.-H. Kim, and Y.-J. Park, "Optimal design of a wireless power transfer system with multiple self-resonators for an LED TV," IEEE Trans. Consum. Electron., vol. 58, no. 3, pp. 775–780, Aug. 2012.

[2] N. S. Jeong and F. Carobolante, "Wireless charging of a metal-body device," IEEE Trans. Microw. Theory Techn., vol. 65, no. 4, pp. 1077–1086, Apr. 2017.

[3] I. O.-Isasa, K. P. Benli, F. Casado, J. I. Sancho, and D. Valderas, "Topology analysis of wireless power transfer systems manufactured via inkjet printing technology," IEEE Trans. Ind. Electron., vol. 64, no. 10, pp. 7749–7757, Oct. 2017.

[4] S. Mao, J. Zhang, K. Song, G. Wei, and C. Zhu, "Wireless power transfer using a field-enhancing coil and a small-sized receiver with low coupling coefficient," IET power electron., vol. 9, no. 7, pp. 1546–1552, Jun. 2016.

[5] D. Ahn and S. Hong, "A study on magnetic field repeater in wireless power transfer," IEEE Trans. Ind. Electron., vol. 60, no. 1, pp. 360–371, Jan. 2013.

[6] K. Lee and S. H. Chae, "Power transfer efficiency analysis of intermediate-resonator for wireless power transfer," IEEE Trans. Power Electron., vol. 33, no. 3, pp. 2484–2493, Mar. 2018.

[7] C. K. Lee, W. X. Zhong, and S. Y. R. Hui, "Effects of magnetic coupling of nonadjacent resonators on wireless power domino-resonator systems," IEEE Trans. Power Electron., vol. 27, no. 4, pp. 1905–1916, Apr. 2012.

[8] O. Karaca, F. Kappeler, D. Waldau, and R. M. Kennel, "Eigenmode analysis of a multiresonant wireless energy transfer system," IEEE Trans. Ind. Electron., vol. 61, no. 8, pp. 4134–4141, Aug. 2014.

[9] M. Ishihara, K. Umetani, and E. Hiraki, "Automatic resonance frequency tuning method for repeater in resonant inductive coupling wireless power transfer systems," in Proc. 2018 Int. Power Electron. Conf. (IPEC-Niigata 2018-ECCE ASIA), 2018, pp. 1610–1616.

[10] R. Huang, B. Zhang, D. Qiu, and Y. Zhang, "Frequency splitting phenomena of magnetic resonant coupling wireless power transfer," IEEE Trans. Magn., vol. 50, no. 11, 8600204, Nov. 2014.

[11] W.-Q. Niu, J.-X. Chu, W. Gu, and A.-D. Shen, "Exact analysis of frequency splitting phenomena of contactless power transfer systems," IEEE Trans. Circuits Syst. I, Reg. Papers, vol. 60, no. 6, pp. 1670–1677, Jun. 2013.

[12] W.Zhang, S.-C. Wong, C. K. Tse, and Q. Chen, "Analysis and comparison of secondary series- and parallel-compensated inductive power transfer systems operating for optimal efficiency and load-independent voltage-transfer ratio," IEEE Trans. Power Electron., vol. 29, no. 6, pp. 2979–2990, Jun. 2014.

[13] A. Trigui, S. Hached, F. Mounaim, A. C. Ammari, and M. Sawan, "Inductive power transfer system with self-calibrated primary resonant frequency," IEEE Trans. Power Electron., vol. 30, no. 11, pp. 6078–6087, Nov. 2015.

[14] R. Mai, Y. Liu, Y. Li, P. Yue, G. Cao, and Z. He, "An active-rectifier-based maximum efficiency tracking method using an additional measurement coil for wireless power transfer," IEEE Trans. Power Electron., vol. 33, no. 1, pp. 716–728, Jan. 2018.

[15] J. Osawa, T. Isobe, and H. Tadano, "Efficiency improvement of high frequency inverter for wireless power transfer system using a series reactive power compensator," in Proc. 2017 IEEE 12th Int. Conf. on Power Electron. and Drive Syst. (PEDS), 2017, pp. 992–998.

[16] Y. Lim, H. Tang, S. Lim and J. Park, "An adaptive impedance-matching network based on a novel capacitor matrix for wireless power transfer," IEEE Trans. Power Electron., vol. 29, no. 8, pp. 4403–4413, Aug. 2014.

[17] Y. Endo and Y. Furukawa, "Proposal for a new resonance adjustment method in magnetically coupled resonance type wireless power transmission," in Proc. 2012 IEEE MTT-S Int. Microw. Workshop Series on Innovative Wireless Power Transmission: Tech., Syst., and Appl. (IMWS-IWPT), 2012, pp. 263–266.

[18] D.-W. Seo, J.-H. Lee, and H.-S. Lee, "Optimal coupling to achieve maximum output power in a WPT system," IEEE Trans. Power Electron., vol. 31, no. 6, pp. 3994–3998, Jun. 2016.

[19] X. Dai, X. Li, Y. Li, and A. P. Hu, "Impedance matching range extension method for maximum power transfer tracking in IPT system," IEEE Trans. Power Electron., vol. 33, no. 5, pp. 4419–4428, May 2018.

[20] Z. Huang, S.-C. Wong, and C. K. Tse, "Control Design for Optimizing Efficiency in Inductive Power Transfer Systems," IEEE Trans. Power Electron., vol. 33, no. 5, pp. 4523–4534, May 2018.

[21] K. Colak, E. Asa, M. Bojarski, D. Czarkowski, and O. C. Onar, "A novel phase-shift control of semibridgeless active rectifier for wireless power transfer," IEEE Trans. Power Electron., vol. 30, no. 11, pp. 6288–6297, Nov. 2015.